JOURNAL OF SPACECRAFT AND ROCKETS
Vol. 31, No. 2, March–April 1994

Navier-Stokes Solver for Hypersonic Flow over a Slender Cone

Chang-Sheng Tai*
Chung Cheng Institute of Technology, Ta-Shi, Taoyuan, Taiwan, Republic of China
and
Ar-Fu Kao†
Armour Research and Development Center, Nan-Tou, Taiwan, Republic of China

A full Navier-Stokes code has been developed for predicting the aerodynamic properties of slender cones. This code can simulate an entire flowfield of slender cones, such as boundary layer and vortices. An explicit upwind flux-difference-split scheme combined with a multistage method has been implemented for solving the steady axisymmetric full Navier-Stokes equations. Experimental data are found to be in good agreement with the code predictions. This code can be extended to a multidimensional program for simulating the three-dimensional practical problem.

Nomenclature

e = internal energy, J/kg
H = total enthalpy, J
M = Mach number
Pr = Prandtl number
p = pressure, N/m^2
R_B = model radius of the slender cone base, m
Re = Reynolds number
T = temperature, K
u, v, w = velocity components in x, y, z directions, m/s
V = streamwise velocity, m/s
x, y, z = Cartesian coordinates
β = deflection angle of shock wave, deg
γ = ratio of specific heats
θc = half-angle of cone, deg
μ = viscosity, kg/s•m
ρ = density, kg/m^3
τ = shear stress, N/m^2

Subscripts

x, y, z = partial derivatives
∞ = freestream

Superscripts

i = inviscid part
μ = viscous part
$\sim$ = dimensional quantity
$\_$ = averaged quantity

Introduction

AERODYNAMICISTS have been investigating the supersonic and hypersonic flowfields around slender cones for years.[1-9] Most of the studies have been performed by experiment, due to the complexity of this problem and limitations in computer capability. However, a few simple analytical and numerical simulations have also been published at a later stage.[10] The wide Mach number range of the re-entry flight profile and the relatively small and limited capabilities of hypersonic test facilities have led to a greater reliance on comprehensive computational methods for vehicle design than on those methods that have been previously used in any other aerodynamic vehicle development program. In this paper, an improved numerical approach has been applied for simulating the complete flowfield, which includes the base region of a slender cone at hypersonic speed. An explicit multistage upwind flux-difference-split scheme (Roe's scheme),[11,12] coupled with Tannehill and Mugge's polynomial correlations,[13] has been developed for solving the steady full Navier-Stokes equations. Discontinuities captured by this upwind method are more sharp than those captured by the conventional central-difference method because the upwind method introduces a minimum amount of dissipation needed to prevent oscillations. This technique can accurately simulate the entire flowfield of a slender cone, including vortices, and therefore it is capable of being applied to numerical simulations in various cone configurations, freestream Mach numbers, and Reynolds numbers.[14]

Calculations have been made for the entire flowfield of a slender cone. Those calculations have been compared with experiments conducted by Bulmer,[15] who had a cone with a half-angle of 9 deg at Mach number 16 and freestream Reynolds number between 3.0×10^5 and 5.76×10^6. The base pressure obtained by the present computation has been shown to be in good agreement with the experimental measurements.

Computational Grid

In this paper, the flowfield of a flight vehicle is simulated with a spherical bluntness ratio R_N/R_B of 0.05, and a cone half-angle θ_c of 9 deg. The schematic of the vehicle is presented in Fig. 1. The grids for the study are 161 × 81 cells, and they are generated by the algebraic method. Figure 2 is the expanded view of the grid near the model. The stretching transformation clusters near the wall of the cone come from the family of general stretching transformation proposed by Anderson et al.[16]

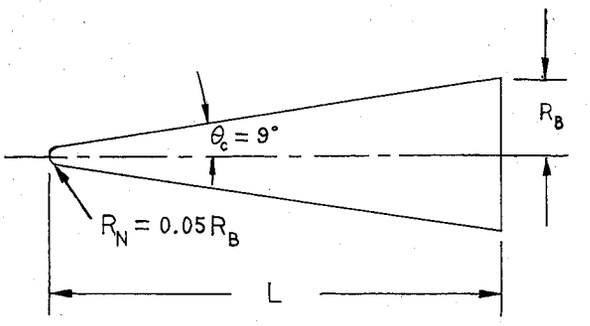

Fig. 1 Slender cone configuration.

Received Feb. 18, 1992; revision received Dec. 28, 1992; accepted for publication Dec. 28, 1992.

*Associate Professor, Department of Aeronautical Engineering.
†Research Scientist.

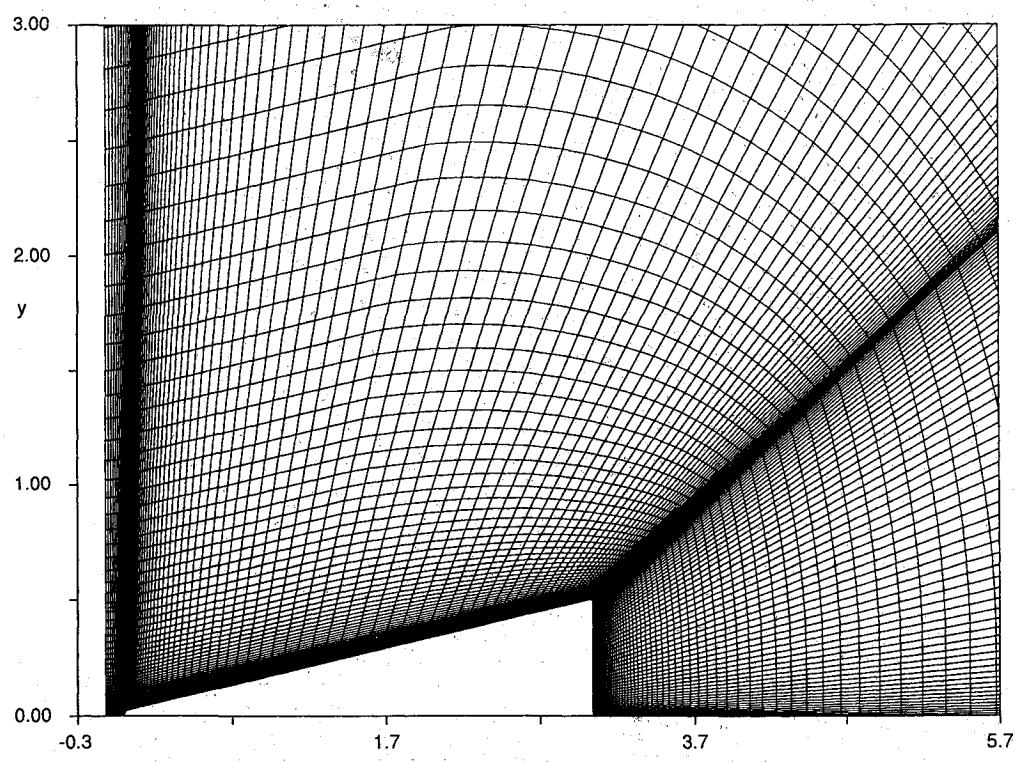

Fig. 2 Expanded view of grids near the model.

Governing Equations

The objective of this paper is to compute the entire flowfield of a slender cone with a wide range of flight Mach numbers. The present work simulates the axisymmetric geometry, however, the code has been developed to solve three-dimensional full Navier-Stokes equations. The governing equation can be written in a strong conservation form as

$$\frac{\partial \bar{U}}{\partial t}+\frac{\partial \bar{F}}{\partial x}+\frac{\partial \bar{G}}{\partial y}+\frac{\partial \bar{H}}{\partial z}=0 \tag{1}$$

where x is the streamwise coordinate, y and z are the radial coordinates, and

$$\bar{U}=\begin{bmatrix}\rho\\ \rho u\\ \rho v\\ \rho w\\ \rho E\end{bmatrix},\quad \bar{F}=\begin{bmatrix}\rho u\\ \rho u^2+p-\tau_{xx}\\ \rho uv-\tau_{xy}\\ \rho uw-\tau_{xz}\\ \rho uH^*-u\tau_{xx}-v\tau_{xy}-w\tau_{xz}+q_x\end{bmatrix}$$

$$\bar{G}=\begin{bmatrix}\rho v\\ \rho uv-\tau_{xy}\\ \rho v^2+p-\tau_{yy}\\ \rho vw-\tau_{yz}\\ \rho vH^*-u\tau_{xy}-v\tau_{yy}-w\tau_{yz}+q_y\end{bmatrix}$$

$$\bar{H}=\begin{bmatrix}\rho w\\ \rho uw-\tau_{xz}\\ \rho uv-\tau_{yz}\\ \rho w^2+p-\tau_{zz}\\ \rho wH^*-u\tau_{xz}-v\tau_{yz}-w\tau_{zz}+q_z\end{bmatrix}$$

where $H^*=E+P/\rho$ is the total enthalpy. The viscous stresses and the heat fluxes are defined as usual.

The equations are completed by the equation of state and constitute relations for the coefficient of viscosity and the conductivity. The coefficients of viscosity in the preceding equations are obtained from Sutherland's law. The conductivity is obtained by assuming a constant Prandtl number ($Pr=0.72$ for air). The polynomial correlations of Anderson[17] have been widely applied to modify the state of equation in the hypersonic flow simulation. In this paper the thermodynamic properties are obtained by using the correlation equations,

$$\tilde{p}=\tilde{p}(\tilde{e},\tilde{\rho}),\qquad \tilde{\gamma}=\tilde{\gamma}(\tilde{e},\tilde{\rho}),\qquad \tilde{T}=\tilde{T}(\tilde{p},\tilde{\rho}) \tag{2}$$

For more details refer to Ref. 13.

The Navier-Stokes equations can be expressed in an integral form as a finite volume with an enclosing surface. The integral form can be expressed in terms of the changes in the average state U in the finite volume.[18,19] The surface integral becomes a sum of fluxes over the six faces of a hexahedron. Equation (1) can be written in the normal flux form as

$$\Delta\tilde{V}\frac{\mathrm{d}\bar{U}}{\mathrm{d}t}+\sum_{n=1}^{6}F_n\Delta A_n=0 \tag{3}$$

where F_n is the flux normal to the cell surface, $F_n=\bar{F}\cos\alpha+\bar{F}\cos\beta+\bar{F}\cos\gamma$, and $\cos\alpha$, $\cos\beta$, and $\cos\gamma$ are the direction cosine of the nth face.

Boundary Conditions

To impose the no-flow-through boundary condition along the surface of the slender cone, we first rewrite the boundary integral of Eq. (1) in terms of the flux velocity defined by $uA_x+vA_y+wA_z$. Then we set the normal flux velocity for the control volume along the cone surface equal to zero.

In the far field, a characteristic analysis based on Riemann invariants is used to determine the values of the flow variable on the outer boundary of the grid. This analysis correctly accounts for wave propagation in the far field, which is important for rapid convergence to a steady state.

Numerical Methods

The use of upwind difference schemes for solving the Euler and Navier-Stokes equations is becoming popular for several reasons.[11,20] For example, upwind schemes have natural numerical dissipation, better stability properties, and more accurate results. Furthermore, if techniques such as multigrid strategy, vector and parallel architectures, and local grid refinement are to be used, then the explicit scheme is preferred. So the explicit multistage Roe's flux-difference-splitting scheme,[11,12,21] which can be applied to the conservation law and can accurately represent the boundary layer, is then chosen as the particular upwind method used here.

Discretizing the conservative form of Eq. (1) is useful for analysis, therefore, Eq. (1) can be written as

$$\frac{dU}{dt} + \frac{1}{\Delta \tilde{V}} \sum_{n=1}^{6} F_n \Delta A_n = 0 \tag{4}$$

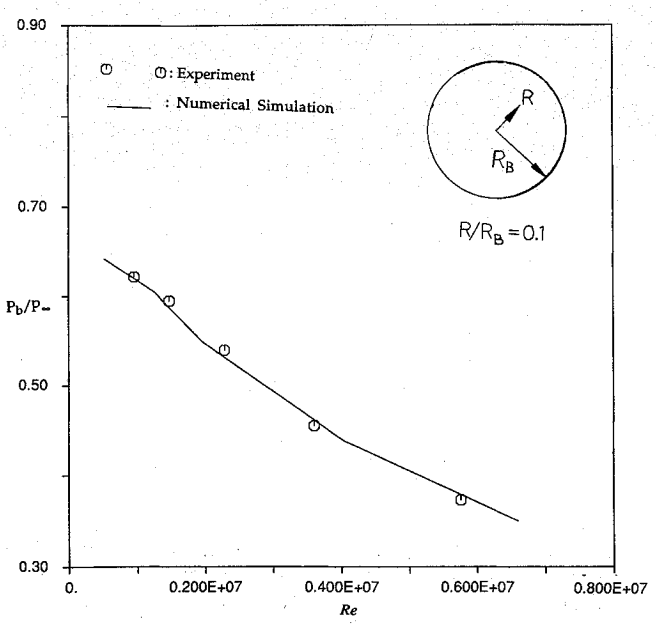

Fig. 3 Comparison of calculated and measured Pb/p_∞ at $R/R_B = 0.1$ for the base region.

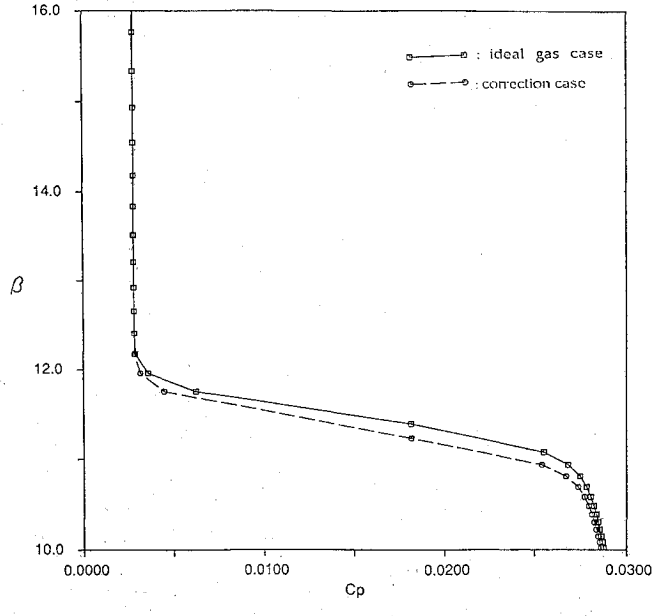

Fig. 4 Comparison of the pressure coefficient Cp profiles between ideal-gas model and corrected-gas model at $\bar{x} = 2.7$, $M_\infty = 16$.

in which the flux vector can be expressed as the sum of an inviscid and a viscous/conductive part:

$$F_n = F_n^i + F_n^\mu \tag{5}$$

The inviscid fluxes are approximated through a flux-splitting scheme (Roe's scheme), and the viscous fluxes are approximated through central differencing.

The basic method of inviscid flux computation is essentially the same for both grid-aligned and grid-independent schemes. It is based on Roe's approximated Riemann solver[22] for the Euler equations:

$$\begin{aligned} F_n^i &= F_n^i(U_R, U_L) \\ &= \tfrac{1}{2}[F_n^i(U_R) + F_n^i(U_L)] - \tfrac{1}{2}|A(U_R, U_L)|(U_R - U_L) \\ &= \tfrac{1}{2}[F_n^i(U_R) + F_n^i(U_L)] - \tfrac{1}{2}|A(\hat{U})|\Delta U \\ &= \tfrac{1}{2}[F_n^i(U_R) + F_n^i(U_L)] - \tfrac{1}{2}R|\Lambda|\Delta V \end{aligned} \tag{6}$$

where U_L and U_R are the left and right interface states, and matrix A is the Jacobian of $F(U)$; $|A(U)|$ denotes the matrix with the same eigenvectors as A and the absolute value of its eigenvalues. The eigenvalues of A are the characteristic speeds $\hat{U} - \hat{C}$, $\hat{U}$, $\hat{U}$, $\hat{U}$, $\hat{U} + \hat{C}$, where the carets refer to Roe averages. Matrix R is composed of the right eigenvector A, and $\Delta V = R^{-1}\Delta U$. Matrix Λ is the diagonal matrix of these eigenvalues; $|\Lambda|$ is computed from the diagonal matrix of absolute characteristic speed. The modified absolute speeds enforce the entropy condition that eliminates expansion shocks and insures a smooth transition from subsonic to supersonic.

Results and Discussion

Several mainstream speeds are solved in this paper, including supersonic and hypersonic flows over a slender cone. A series of those are used for comparison with experimental results. The flow conditions for investigation in this study are hypersonic flows at $M_\infty = 16$, and the cone boundary layers near the base region are laminar for Reynolds number between 0.951 and 5.76×10^6. The base pressure P_b at the base radial location ($R/R_B = 0.1$) was measured by Bulmer.[7]

Figure 3 shows the base pressure data, normalized by freestream static pressure (p_∞), in terms of the freestream Reynolds number. The calculated slope of the pressure ratio is in good agreement with the experiment.

Figure 4 shows the variation of pressure coefficient in the y direction at $\bar{x} = 2.7$ for both cases, the ideal-gas model and the gas model with specific ratio γ and temperature corrected, at freestream Mach number $M_\infty = 16$. The computed deflection angle of the shock wave for the ideal-gas model is 11.5. It is higher than that of 11.0 found in chart 5 of Ref. 23 at $M_\infty = 16$ and $\theta_c = 9$ deg. This is because the viscous flow, studied currently, makes the effective angle higher than the geometric angle. The deflection angle of the corrected case is lower than that of the ideal-gas case. This may be attributed to the phenomenon such as gas molecule dissociation that has already been considered in the corrected case.

Figures 5a–5c show the Mach number contours, pressure contours, and temperature contours, respectively, over the slender cone at $M_\infty = 16$, $Re_\infty = 6.0 \times 10^6$, and $T_\infty = 200$ K. The upper parts of these figures are corrected by the correlation polynomial, and the lower parts are shown for the ideal-gas cases. Figure 6 shows the temperature contours at $M_\infty = 3$ with the same Reynolds number and freestream temperature as in the cases shown in Fig. 5.

From Figs. 5 and 6, two observations are obtained. One is that the Mach number contours and the pressure contours are similar for two cases (ideal gas and correlation polynomial correction) at any freestream Mach number. The other one is the stronger effect on temperature contours for different Mach numbers; such a conclusion had been obtained years ago.[17]

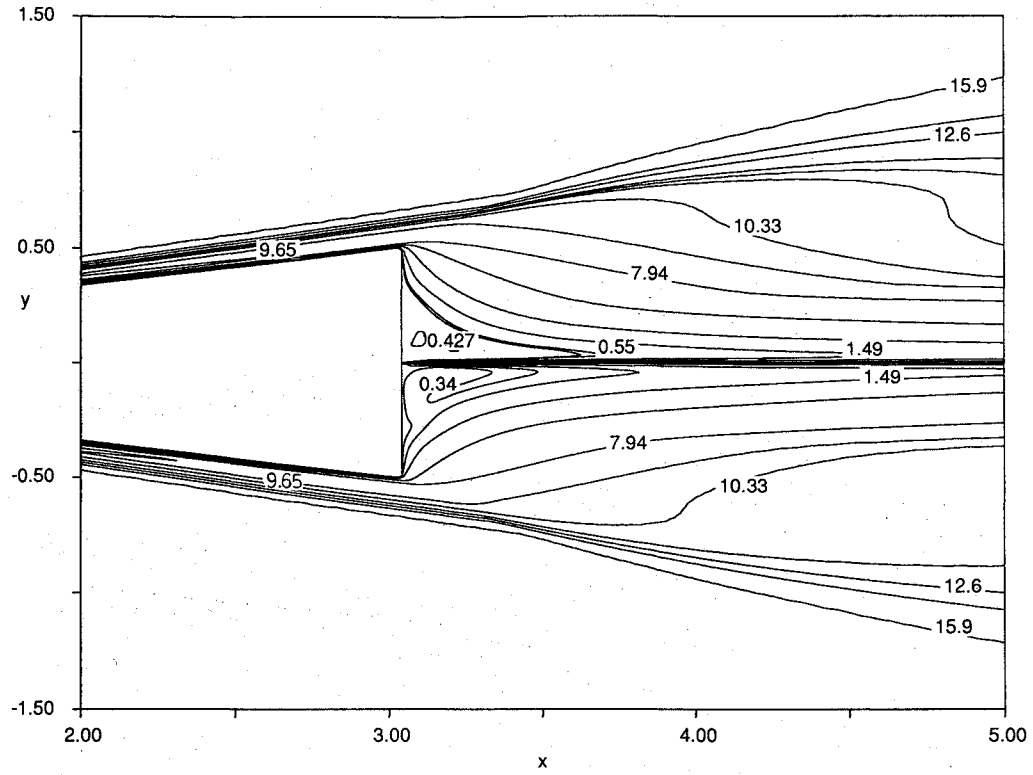

Fig. 5a Comparison of the Mach number contours between corrected-gas model (upper part) and ideal-gas model (lower part) at $M_\infty = 16$.

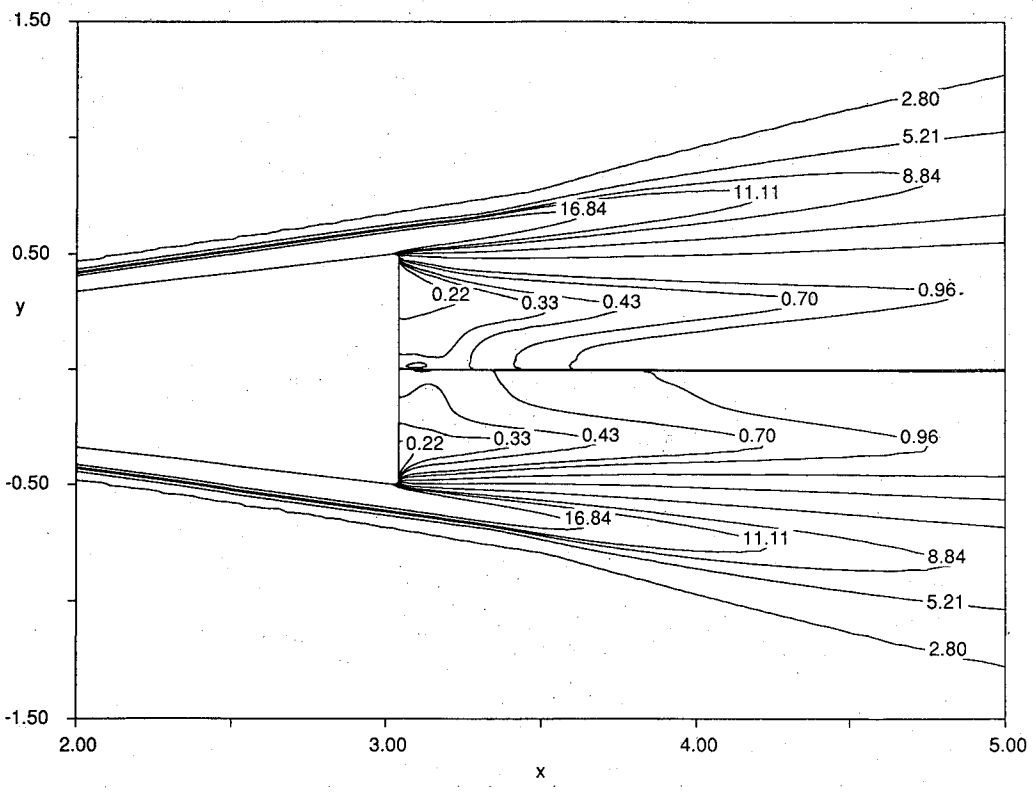

Fig. 5b Comparison of the pressure contours between corrected-gas model (upper part) and ideal-gas model (lower part) at $M_\infty = 16$.

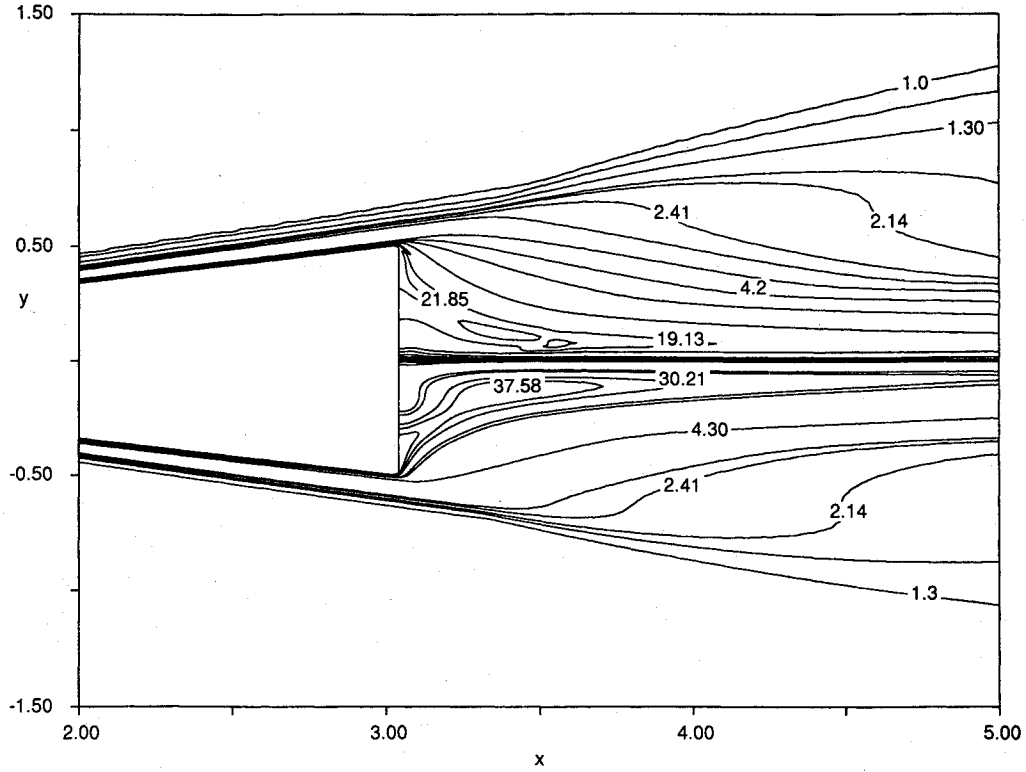

Fig. 5c Comparison of the temperature contours between corrected-gas model (upper part) and ideal-gas model (lower part) at $M_\infty = 16$.

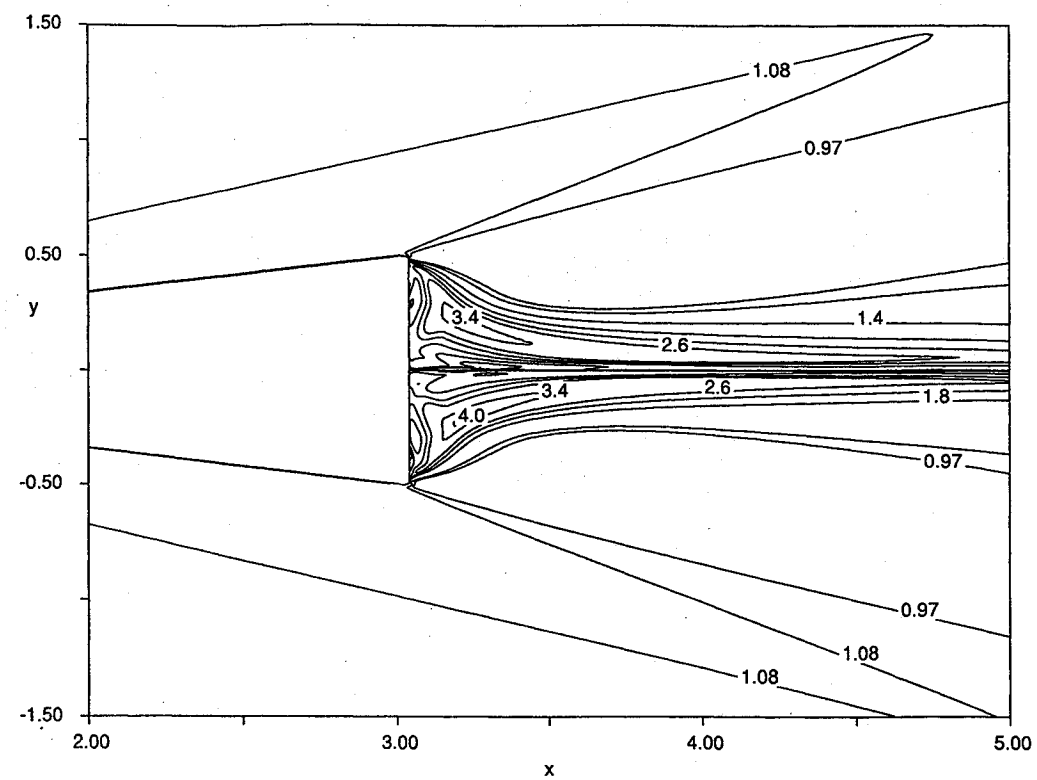

Fig. 6 Comparison of the temperature contours between corrected-gas model (upper part) and ideal-gas model (lower part) at $M_\infty = 3$.

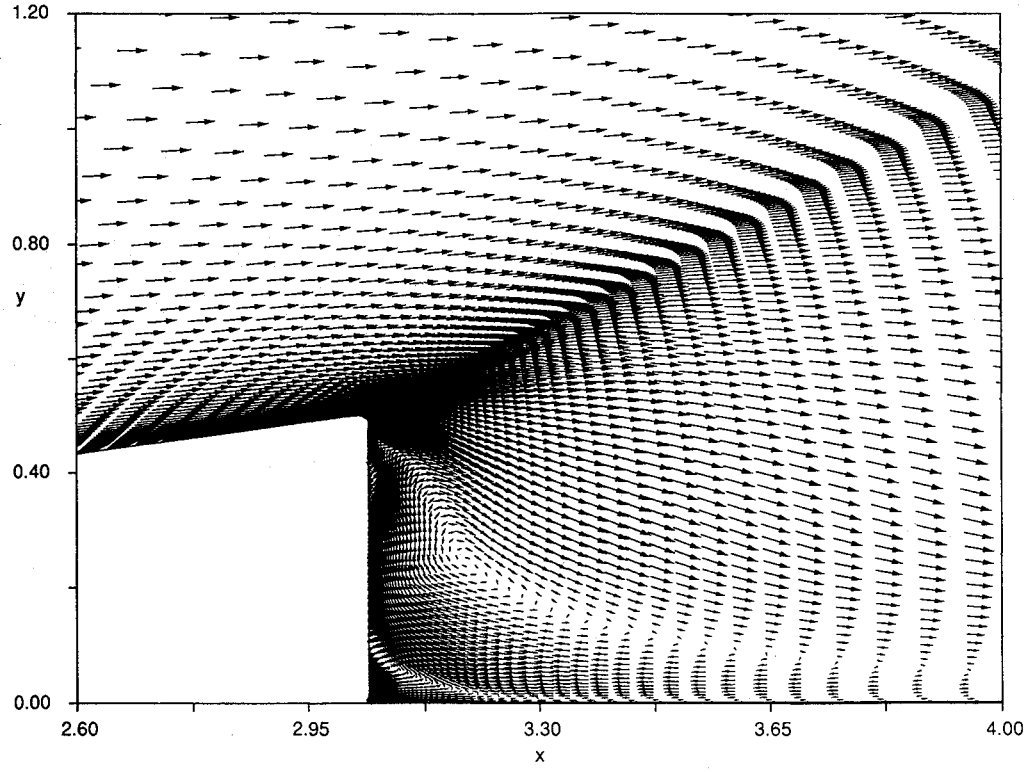

Fig. 7 Velocity vector field near the base region, $M_\infty = 3$.

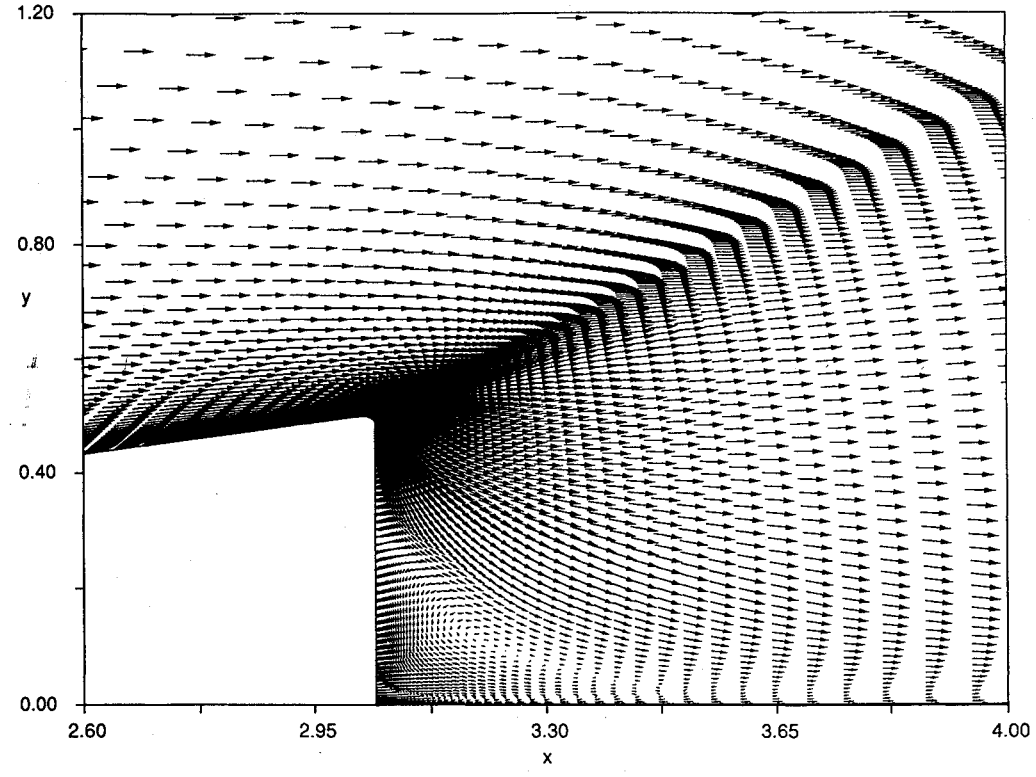

Fig. 8 Velocity vector field near the base region, $M_\infty = 16$.

Figures 7 and 8 show the velocity vector field at $M_\infty = 3$ and 16, respectively. Each vector shows the magnitude and the direction of the velocity at that point. The boundary layer near the wall is observed clearly. The phenomena of the base zone are very sophisticated. From Figs. 7 and 8, coupled vortices at the base region are observed. The velocity vectors show the complex phenomena of the interaction of vortices. It is also found that their directions are opposite and the strength of the primary vortex is stronger than the secondary vortex. At $M_\infty = 16$ the primary vortex is so strong that the velocity profile far from the base region is very different from the velocity profile at Mach number 3.

A comparison of the streamline contours near the base region is shown in Fig. 9. The upper part is for $M_\infty = 3$ and the lower part is for $M_\infty = 16$. Figure 9 shows that, as the freestream Mach number increases, the vortex velocity vectors increase in magnitude, but the vortices' regions become more restricted.

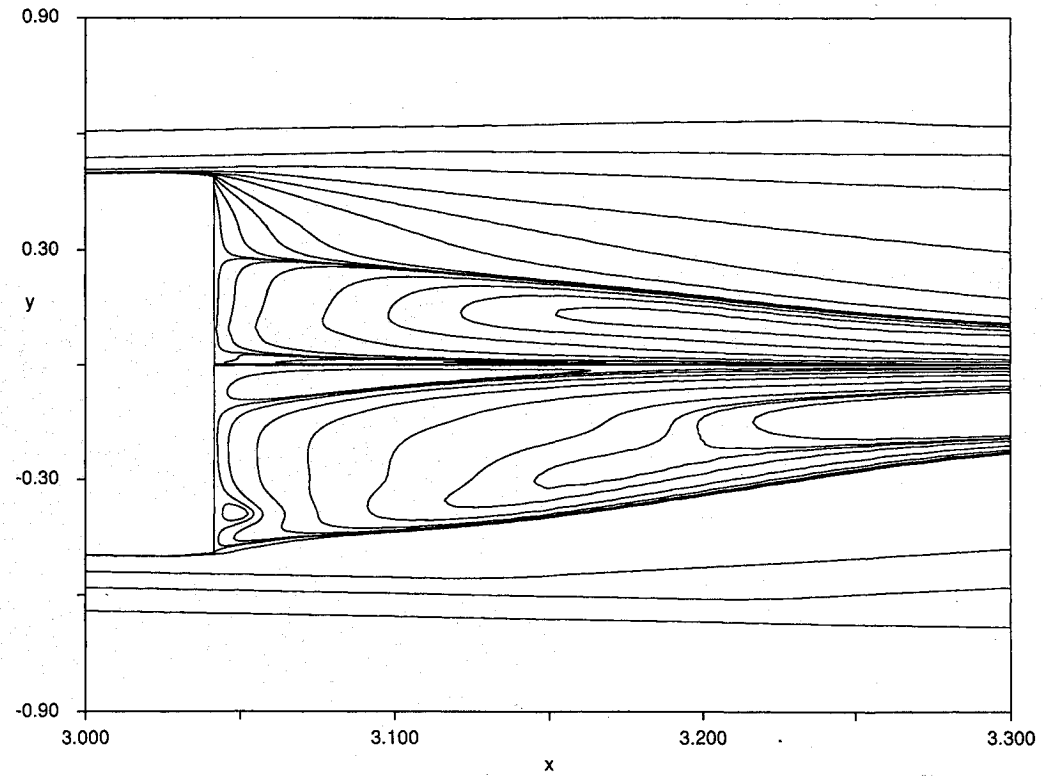

Fig. 9 Comparison of the streamline contours near the base region, the freestream Mach number $M_\infty = 3$ (upper part) and $M_\infty = 16$ (lower part).

Conclusions

The supersonic and hypersonic laminar flow over a slender cone has been numerically calculated. The full Navier-Stokes equations were solved by an explicit multistage, upwind flux-difference-split scheme (Roe's scheme).

An algorithm has been presented for computing a wide range of freestream Mach numbers and Reynolds numbers. Numerical simulations have been made for Mach number 16 and Reynolds numbers between 0.951 and 5.76×10^6. The base pressures obtained by the present computation and the experimental measurements are found to be in good agreement. This provides the necessary validation of the newly developed code.

Considering the future development of the multigrid strategy, the application of the vector and parallel architectures, and the implementation of local grid refinement, the code is designed to have the good performance of extension. Numerical approaches, including the high-order total variation diminishing scheme, the appropriate turbulent model, and the multigrid strategy, can be added to this code to obtain more accurate results. The code must extend to a really three-dimensional solver to solve the problem with angle of attack. Several results obtained by the modification mentioned earlier have been found to be a good match for the experimental data.

Acknowledgments

The authors are grateful to the National Science Council of the Republic of China for financial support under Contract NSC-82-04D1-E-014-007. Fruitful discussions concerning several aspects of the work with C. H. Tai are acknowledged.

References

[1]Lees, L., "Hypersonic Wakes and Trails," *AIAA Journal*, Vol. 2, No. 3, 1964, pp. 417–428.

[2]Zakkay, V., and Cresci, R. J., "An Experimental Investigation of the Near Wake of a Slender Cone at $M = 8$ and 12," *AIAA Journal*, Vol. 4, No. 1, 1966, pp. 41–46.

[3]Muntz, E. P., and Softley, E. J., "A Study of Laminar Near Wakes," *AIAA Journal*, Vol. 4, No. 6, 1966, pp. 961–968.

[4]Murman, E. M., "Experimental Studies of a Laminar Hypersonic Cone Wake," *AIAA Journal*, Vol. 7, No. 9, 1969, pp. 1724–1730.

[5]Cassanto, J. M., Schiff, J., and Softley, E. J., "Base Pressure Measurements on Slender Cones with Domed Afterbodies," *AIAA Journal*, Vol. 7, No. 8, 1969, pp. 1607–1609.

[6]Cassanto, J. M., Rasmussen, N. S., and Coats, J. D., "Correlation of Free-Flight Base Pressure Data for $M = 4$ to $M = 19$," *AIAA Journal*, Vol. 7, No. 6, 1969, pp. 1154–1157.

[7]Bulmer, B. M., "Study of Base Pressure in Laminar Hypersonic Flow: Re-Entry Flight Measurements," *AIAA Journal*, Vol. 13, No. 10, 1975, pp. 1340–1348.

[8]Lin, A., and Rubin, S. G., "Three-Dimensional Supersonic Viscous Flow over a Cone at Incidence," *AIAA Journal*, Vol. 20, No. 11, 1982, pp. 1500–1507.

[9]Dolling, D. S., and Gray, W. K., "Experimental Study of Supersonic Turbulent Flow on a Blunted Axisymmetric Body," *AIAA Journal*, Vol. 24, No. 5, 1986, pp. 793–799.

[10]Tannehill, J. C., Buelow, P. C., Ievalts, J. O., and Lawrence, S. L., "Three-Dimensional Upwind Parabolized Navier-Stokes Code for Real Gas Flows," *Journal of Spacecraft and Rockets*, Vol. 27, No. 2, 1990, pp. 150–159.

[11]Roe, P. L., "Approximate Riemann Solvers, Parameter Vector, and Difference Schemes," *Journal of Computational Physics*, Vol. 43, Oct. 1981, pp. 357–372.

[12]Van Leer, B., Thomas, J. L., Roe, P. L., and Newsome, R. W., "A Comparison of Numerical Flux Formulas for the Euler and Navier-Stokes Equations," AIAA Paper 87-1104, June 1987.

[13]Tannehill, J. C., and Mugge, P. H., "Improved Curve Fits for the Thermodynamic Properties of Equilibrium Air Suitable for Numerical Computation Using Time-Dependent or Shock-Capturing Methods," NASA CR-2470, Oct. 1974.

[14]Tai, C. H., and Tian, Y. L., "The Numerical Simulation of Axisymmetrical Spinning Projectile," *NIXT'91, Third International Symposium on Explosives Technology and Ballistics* (Pretoria, South Africa), pp. 679–689.

[15]Bulmer, B. M., "Study of Base Pressure in Laminar Hypersonic Flow: Re-Entry Flight Measurements," *AIAA Journal*, Vol. 13, No. 10, 1975, pp. 1340–1348.

[16]Anderson, D. A., Tannehill, J. C., and Pletcher, R. H., *Computational Fluid Mechanics and Heat Transfer*, McGraw-Hill, New

York, 1984, pp. 247–252.

[17]Anderson, J. D., Jr., *Hypersonic and High Temperature Gas Dynamics*, McGraw-Hill, Singapore, 1989, pp. 460, 461, 510.

[18]Abgrall, R., "Generalization of the Roe Scheme for Calculating Flow of Mixed and Variable Concentrations," *La Recherche Aerospatiale*, Vol. 1988-6, June 1988, pp. 32–43.

[19]Schmidt, J. W., and Turkel, E., "Numerical Solution of the Euler Equations by a Finite-Volume Method Using Runge-Kutta Time-Stepping Schemes," AIAA Paper 81-1259, June 1981.

[20]Van Leer, B., Tai, C. H., and Powell, K., "Design of Optimally Smoothing Multi-Stage Schemes for the Euler Equations," AIAA Paper 89-1933, June 1989.

[21]Hirsch, C., *Numerical Computation of Internal and External Flow*, Vol. 2, Wiley-Interscience, New York, 1989, pp. 127, 409, 460–469.

[22]Van Leer, B., "Upwind-Difference Problems Governed by the Euler Equations," *Lectures in Applied Mathematics*, Vol. 22, 1985, pp. 327–336.

[23]Anon., "Equations, Tables, and Charts for Compressible Flow," Ames Aeronautical Lab., NACA-R-1135, 1953.